

# Dynamical Global Downscaling of Global Reanalysis

Kei Yoshimura<sup>1,2</sup> and Masao Kanamitsu<sup>1</sup>

<sup>1</sup>Scripps Institution of Oceanography, University of California, San Diego

<sup>2</sup>Institute of Industrial Science, The University of Tokyo

Submitted to Monthly Weather Review

Submitted on 2007/06/08

Revision submitted on 2007/11/02

Corresponding author:

Kei Yoshimura ([klyoshimura@ucsd.edu](mailto:klyoshimura@ucsd.edu)),

CRD/SIO/UCSD MC0224, 9500 Gilman Dr., La Jolla, CA92093-0224, USA

## ABSTRACT

Aiming at producing higher resolution global reanalysis datasets from coarse resolution reanalysis, a global version of the dynamical downscaling using a global spectral model (GSM) is developed. A variant of spectral nudging, the modified form of scale-selective bias correction (SSBC) developed for regional models is adopted. The method includes; 1) nudging of temperature in addition to the zonal and meridional components of winds, 2) nudging to the perturbation field rather than to the perturbation tendency, 3) no nudging and correction of the humidity. The downscaling experiment was performed using T248L28 (about 50 km resolution) global model, driven by NCEP/NCAR Reanalysis 2 (T62L28 resolution, about 200 km resolution) during 2001. Evaluation with high-resolution observations showed that the monthly averaged global surface temperature and daily variation of precipitation were much improved. Over North America, surface wind speed and temperature are much better, and over Japan, the diurnal pattern of surface temperature is much improved, as are wind speed and precipitation, but not humidity. Three well-known synoptic/sub-synoptic scale weather patterns over the USA, Europe, and Antarctica were shown to become more realistic. This study suggests that the global downscaling is a viable and economical method to obtain high-resolution reanalysis without re-running a very expensive high-resolution full data assimilation.

## 1. Introduction

Reanalysis is now an indispensable dataset for climate studies. It provides analysis of a variety of variables, which are internally consistent within the framework of the numerical model used in the data assimilation. However, its coarse spatial resolution has been problematic for various application studies, such as the regional impact of climate change on agriculture (Fuhrer et al., 2006), river flows (Wilby et al., 1999 and Miller et al., 2003), terrestrial water and energy cycle (Dirmeyer et al., 2006), water resources estimation with anthropogenic impacts (Oki and Kanae, 2006, Lehner et al., 2006), and many others.

The coarseness of the reanalysis resolution is mainly due to the computational burden. For example, one analysis by a typical data assimilation requires computer time approximately equivalent to a 4-5 day forecast. Since reanalysis involves analyzing a very long period of data (40 plus years) in a reasonable time (normally within 3-5 years), limiting the analysis resolution is unavoidable.

One approach to obtain high resolution analysis is the use of regional data assimilation. NCEP (National Centers for Environmental Prediction) recently performed regional reanalysis over the United States for the period 1979 to present using 32 km resolution (Mesinger et al., 2006). European countries are also working together on a similar project (EURRA, 2005). While this approach is feasible, such efforts are limited to a small number of countries and institutions that have advanced data assimilation systems and ample computer power.

Dynamical downscaling is an alternative to regional data assimilation. As pointed out by von Storch et al. (2000), dynamical downscaling with the spectral

nudging technique is considered a “poor person’s data assimilation technique.” Some comparisons between regional data assimilation and dynamical downscaling have been studied by Kanamaru and Kanamitsu (2007a). It was concluded that the dynamical downscaling with higher spatial resolution (10 km) has an advantage over the coarser resolution (32 km) regional data assimilation. Part of the reason is that the current data assimilation system is incapable of effectively utilizing high-density near-surface observations, and places more weight on the initial guess produced by the regional high-resolution numerical model. In spite of its economical merit, a regional climate model, and accordingly the downscaling, is inherently mathematically ill-posed due to specified lateral boundary values, which result in noises and instabilities that propagate into the interior of the domain and contaminate the downscaled analysis. Thus, for the purpose of examining the effect of the lateral boundary in the RCM-downscaling, a downscaling without any lateral boundary is desirable.

Under the GEWEX (Global Energy and Water Cycle Experiment), as a transferability intercomparison project, Rockel et al. (2006) proposed a comparison of regional simulations with fixed model parameterizations over several globally-distributed domains to test the model performance and to improve model parameterizations. The project targets regional models, but if similar experiments can be performed using a global model, this could be ideal for regional comparison since the simulation would not be contaminated by lateral boundaries. The global downscaling can also be more economical than running the regional model at many locations because the global model eliminates the sizeable overheads required to run the regional model separately at multiple locations.

In this study, a global version of the dynamical downscaling is developed. The system uses global spectral model and spectral nudging, and produces finer resolution global datasets from 200 km resolution reanalysis. For this purpose, a modified version of the scale-selective bias correction (Kanamaru and Kanamitsu, 2007a), is developed. The major objective of this paper is to demonstrate that a “global high-resolution” version of the NCEP global Reanalysis can be produced with relatively low computer cost.

A different type of global downscaling was recently conducted by Ghan et al. (2006). They downscaled a GCM (general circulation model) simulation with a physically based subgrid orography scheme over global terrain for a multi-decadal period. In their method, surface variables in each coarse grid cell were redistributed into finer subgrids taking into account the elevation effect, but with rather crude airflow dynamics within a grid, and an offline-mode of a land surface model was driven by these surface variables. Their method is not fully dynamical downscaling, but rather a practical and computationally inexpensive approach to global downscaling.

This paper is outlined as follows. Section 2 describes a global version of the spectral nudging technique, specifically, the modification of the scale-selective bias correction method, and the results of the preliminary short-term nudging experiments are shown. Section 3 presents results from a finer longer-term downscaling experiment. The results are evaluated against observations over the globe and over specific regions. Finally, Section 4 provides a summary and conclusions.

## 2. Method

### *a. Modification of SSBC for a global spectral model*

The scale-selective bias correction (SSBC) scheme for a regional spectral model (RSM) developed by Kanamaru and Kanamitsu (2007a; KK07 hereafter) was modified for the global spectral model (GSM), and was used as a base for this study. The GSM is based on the medium range forecast (MRF) model developed at NCEP for making operational analysis and predictions (see Caplan et al, 1997), and was further improved at the Scripps Institution of Oceanography (SIO). The RSM used by KK07 was also developed at NCEP and improved later at SIO (Kanamitsu et al., 2005). The physical parameterizations used by GSM and RSM are identical and the two models share many other components. The SSBC developed for RSM required modification due to differences in the spectral basis functions used in GSM and RSM, as well as to the much wider area coverage that includes the tropics and extra-tropics.

Prior to the downscaling process, the driving reanalysis data were pre-processed; surface pressure was recalculated for higher resolution topography in the high-resolution global model with the hydrostatic relationship, and temperature, humidity, and wind fields were vertically interpolated to the new model sigma levels. This process is basically the same as that of the RSM-SSBC's correction for surface pressure.

In the RSM, the sine and cosine series for both  $x$  - and  $y$ -directions are used as basis functions, and nudging is applied directly to the two dimensional sine and cosine amplitudes. In GSM, the basis function is a spherical harmonics, and the SSBC equivalent of RSM is to apply the nudging to the amplitude of total

wavenumber. However, this implies that the nudging is uniformly applied in the zonal and meridional directions. In reality, it is desirable to nudge differently for the zonal and meridional directions, since the atmospheric long waves tend to have larger scale in east-west than in north-south. For this reason, SSBC for a specified zonal scale is applied at each Gaussian latitude. The advantage of this method compared to nudging in the spherical harmonics function is described in detail in the Appendix (Experiments SP21 and SP42). The equations for nudging using a fully implicit time scheme are written as follows:

$$f_{(\lambda,\phi)} = \sum_{m=-M}^{m=M} A_{(m,\phi)} e^{im\lambda} \quad (1)$$

$$A_{(m,\phi)} = \begin{cases} A_{f(m,\phi)} & (|m| > \frac{2\pi R_E \cos\phi}{L}) \\ \frac{1}{\alpha + 1} (A_{f(m,\phi)} + \alpha A_{a(m,\phi)}) & (|m| \leq \frac{2\pi R_E \cos\phi}{L}) \end{cases}$$

where  $f$  is a physical variable (full field),  $A$  is the Fourier coefficient, and the subscript  $f$  and  $a$  indicate forecast and analysis (driving data), respectively.  $\lambda$ ,  $\phi$ ,  $R_E$ ,  $m$  and  $M$  indicate longitude, latitude, radius of the earth, wavenumber, and the truncation wave number, respectively.  $\alpha$  is a nudging coefficient, and  $L$  is a critical nudging scale where waves longer than  $L$  will be nudged. It should be mentioned that in KK07 the tendency of the perturbation  $\partial F / \partial t$  (perturbation  $F$  is defined as difference between full field and the global analysis,  $F \equiv A_f - A_a$ ) is nudged following:

$$\frac{\partial F}{\partial t}_{new} = \frac{1}{1 + \alpha} \times \frac{\partial F}{\partial t}_{old} \quad (2)$$

but this study nudges the perturbation itself following

$$F_{new} = \frac{1}{1 + \alpha} \times F_{old} \quad (3)$$

The advantage of perturbation field nudging is that the large scale biases can be

more effectively suppressed (Equation 3).

The original SSBC nudged zonal and meridional wind components at all sigma levels towards coarse resolution reanalysis field by using a single weighting coefficient ( $\alpha=0.9$ ). KK07 called this correction UV damping and applied it only to waves whose physical wavelengths are 1000 km or longer. In GSM-SSBC, preliminary experiments were first conducted to find the sensitivities of the simulation to the nudging parameter and to other related parameters, the results being described in the next section and in the Appendix (Experiments ALP05 and ALP2).

In addition, the area average correction in the RSM, which sets the difference between regional area averages of temperature and humidity between reanalysis and downscaling to zero (TQ correction), was replaced to set the difference between the zonal averaged temperature and humidity in reanalysis and downscaling to zero to preserve the meridional gradient of the zonal mean in the reanalysis.

As described below, it was found that the nudging of temperature was necessary to improve simulation in the tropics. Furthermore, the removal of the correction and nudging to moisture was needed to avoid excessive precipitation. Experiments that show the need for additional changes to the regional model nudging procedure for global downscaling are presented in the next subsection.

## *b. Experiments to determine the configuration of nudging*

### **1) Design of the Experiments**

We performed a wide range of sensitivity experiments to find the best

configuration for global downscaling. The experiments were performed to determine:

1. Nudging of temperature and moisture (TEMP, NoQ).
2. Critical meridional and zonal nudging scale (L1000, L1000T, SP21, and SP42).
3. Magnitude of nudging coefficient (ALP05, ALP2).

In addition, integration without any nudging was performed for comparison (FCST). All the experiments were compared against control (CTL), which has the same settings as KK07 except for the addition of zonal mean correction (“UV nudging” with  $\alpha=0.9$  and  $L=2000$  km). See Table 1 for the experiments performed.

These experiments were performed using the same model configurations: the T126 (about 100 km) and 28 sigma levels as a downscaling model; 6-hourly snapshots of prognostic variables from NCEP Reanalysis 2 (R2; Kanamitsu et al., 2002) with a resolution of T62 and 28 levels as a lateral forcing; and 10 day integration starting at the beginning of March 1990 using interpolated Reanalysis as initial conditions. It is noted that the GSM applied in this study used the Noah land surface model and Relaxed Arakawa-Schubert convection scheme (Moorthi and Suarez, 1992) whereas R2 used the OSU land surface model and Simplified Arakawa-Schubert convection scheme (Pan and Wu, 1994).

## **2) Results of the Experiments**

In this section, we concentrate on the temperature and the moisture correction and nudging, which are required for global downscaling. In Figure 1, the power spectra of global kinetic energy at two different sigma levels are shown with those of R2 (up to total wavenumber  $n=62$ ), CTL, TEMP, NoQ, and forecast (FCST) (up to  $n=126$ ). TEMP is the experiment with temperature and moisture nudging,

while in NoQ moisture correction and nudging have been removed from TEMP. The computation of the spherical harmonic spectra by Koshyk and Hamilton (2001) was used to make Figure 1. For the wavenumber less than 20, the power spectra of R2 and CTL are almost identical, indicating that the large-scale nudging is working correctly at both levels (wavenumber 20 corresponds to about 2000 km wavelength at the equator). The FCST spectra deviate from those of R2 at small wavenumbers (ultra long wave scales) after 10 days, indicating the predictability limit due to model error when no nudging is applied.

For the wavenumbers larger than 20, the difference between R2 and CTL is apparent. Particularly for R2, the spectra quickly drop down around wavenumber 40, but CTL keeps its monotonical decrease up to wavenumber 120 at low levels and up to 90 at upper levels. This energy gain between 40 and 120 indicates that the dynamical downscaling is producing reasonable small scales. This can be seen from the nearly constant  $-5/3$  spectra slope particularly at upper levels (Figure 1a). In addition, the spectra of CTL and FCST for wavenumbers larger than 20 stay almost the same, indicating that the large-scale nudging is working and is not significantly impacting the small scale generated by the high-resolution model.

Although the energy spectra seem to be reasonable in CTL, large scale systematic deviation from Reanalysis was found in the tropical stratospheric height field (Figure 2). The error consists of wavenumbers 1 and 2 with its maximum at the equator. From further investigations with a number of sensitivity experiments, it was found that this large scale systematic error was partially created by the global model used in the downscaling. It was also found that, even in the R2 assimilation, a very similar systematic error occurred in the 6 hour forecast guess, which was

corrected by the objective analysis (not shown). Leaving the temperature field unnudged enhanced the bias, amplifying it to 3-4 degrees Kelvin in several days in our global downscaling. The corresponding error in height reached 60-80 m. The cause of this problem might be related to the lack of initialization in the reanalysis, but a study of this error is beyond the scope of this paper. This significant bias in height was not found in previous dynamical downscaling studies using RSMs (Kanamaru and Kanamitsu, 2007a, 2007b) because the horizontal scale of the systematic error was larger than the regional domain, and a correction of area averaged temperature was enough to fix the problem. Another reason might be that the regional downscaling was performed in extra-tropical latitudes where UV damping is sufficient to control the temperature bias.

Based on these analyses, the TEMP experiment, for which the temperature field was nudged together with the wind field, was performed. The vertical profiles of global root mean square difference (RMSD) of geopotential height between the experiments and the forcing (R2) are shown in Figure 3. The values at 500 hPa level are also shown in Table 1. As expected, large-scale systematic bias in the stratosphere was reduced and the global RMSDs are dramatically reduced compared to CTL. The RMSD also decreased in the entire troposphere. The departures of geopotential height from the reanalysis were about 5-10 m at all pressure levels, which is comparable to KK07 (about 2-7 m).

The TEMP experiment was first thought to be the best setting for global downscaling, but it was later discovered that the model significantly overestimated the global precipitation (3.16mm/day in R2, vs. 3.55mm/day in TEMP). The cause of the overestimation is thought to be due to inconsistencies between the moisture

distributions in the Global reanalysis and the model parameterizations (convection, boundary layer and radiation) used in the current GSM, possibly involving an interaction with topography. Based on this supposition, we experimented with the downscaling by entirely removing the nudging and correction of moisture from TEMP (experiment NoQ). It was found that the RMSD stayed as low as the TEMP experiments, but the precipitation was reduced to 3.03mm/day, much closer to the Reanalysis. The very little difference in the RMSD of geopotential height indicates that the specific humidity is more or less passively determined by the dynamical field and nudging of moisture is unnecessary, or even harmful for inconsistent physical and dynamical processes.

Finally, we found that the kinetic energy spectra of TEMP and NoQ are similar to those of CTL (see Figure 1), as is humidity (figure not shown), indicating that the nudging of temperature and no-correction of specific humidity did not cause any dynamical distortion. Even though the experiments were performed with short-term simulations, these high resolution model responses most likely apply to longer integrations. Thus the NoQ setting was chosen as the default for the global downscaling.

The determination of the nudging coefficient, the choice of critical scale, particularly the difference in zonal and meridional directions, and the selection of nudging variables are somewhat empirically made in this study, based on many experiments. The results of those experiments are summarized in the Appendix.

### **3. A 50 km Global Downscaling**

In the previous section, it was confirmed that the large-scale dynamical

features in the reanalysis were successfully retained in the global downscaling. In this section, we examine how downscaled fields improve the fit to observations in a longer downscaling run. For this purpose, a global downscaling by T248 (about 50 km) resolution model was conducted (experiment named T248) for the year 2001. The NoQ nudging scheme was used. The configurations of the experiment match those in the previous section; the number of sigma levels was set to 28 and T62L28 6-hourly NCEP R2 was used for forcing. Considering the spin-up of land surface parameters, the model was run from 1998, but the results for 2001 are shown below.

#### *a. Global Evaluation*

##### **1) Global Temperature compared with CRU**

Figure 4 shows the globally downscaled monthly mean temperature over land compared with the CRU (Climate Research Unit) dataset (version TS 2.1, Mitchell and Jones, 2005). From Figure 4d and 4e, it is found that the Arctic Islands, the extreme northern part of North America, and the eastern part of Siberia are slightly warmer in both R2 and the downscaled analysis. There are slightly cooler biases in Central Africa, the Sahel, and the Amazon Basin. However, there is an obvious improvement associated with the global downscaling due to more realistic surface topography, especially over mountain ranges. The clearest difference can be seen in the Tibetan Plateau and in the Andes, but there are also improvements over the Pacific Coastal Ranges, the Alps, the Ethiopian Plateau, the Mongolian Plateau, and many other locations. Although the other months' results are not shown, the advantage of the downscaling is similar throughout the year.

##### **2) Global Precipitation compared with GPCP and CRU**

In Figure 5, the downscaled analysis and original reanalysis R2 (T62

resolution) monthly precipitation are compared with those of GPCP (Huffman et al., 2001), CRU, and FCST during January and July 2001. Seasonal evolutions over the major continents are clearly simulated well, but they are already well simulated in R2. In both months spatial contrasts associated with topography and coastlines become more apparent in the downscaled analysis, for example, in the Himalaya and Sierra Madre Ranges, the Coast Ranges in British Columbia, and the western coastline of India.

Over oceans, the distribution in the NH in the downscaling agrees with that of GPCP, such as the narrow ITCZ over the Pacific and Atlantic, the wide coverage of large precipitation over the northern Pacific in January and its westward recession in July with less precipitation over the eastern half of the region and Asian Monsoon seasonality. In the SH however, both the downscaled analysis and R2 show erroneous double-ITCZ over the central southern Pacific and the southern Atlantic (near the Atlantic coast of Brazil) in July whereas no such precipitation is found in FCST and GPCP. These errors were not corrected by the downscaling run. Moreover, changing the model physics, such as using other convective parameterizations (Pan and Wu, 1994 or Kain and Fritsch, 1990) instead of RAS or incorporating cloud water physics (Iacobellis and Somerville, 2000), failed to correct the problem (Figures not shown). Therefore, it was concluded that significant large-scale errors existed in the global reanalysis fields causing the erroneous double-ITCZ, but the downscaled model physics and dynamics could not correct the problem. This problem may be avoided by nudging with geographically varying weights based on the accuracy of the reanalysis, which is left for future improvements.

Figure 6 shows the seasonal variation of monthly global mean precipitation compared with GPCP, CRU, and R2. The global mean of downscaled precipitation is in between those of R2 and GPCP throughout the year over the whole globe. The land precipitation is slightly larger than R2 and CRU except in the summer months, but it is within the comparable range (about  $\pm 0.5$  mm/day). It seems that the removal of the moisture nudging allows the moisture to evolve in a consistent manner with the downscaling model physics, producing reasonable amounts of precipitation. As noted earlier, the nudging of the moisture results in excessive precipitation.

Figure 7 shows the global average of temporal correlation coefficients of daily precipitation between the model and 1 degree GPCP during 2001. There are zonal bands of high correlation over mid and high latitudes in both hemispheres, and low correlation over the tropical regions in both Reanalysis and the downscaling as a common feature (not shown). The global average of the correlations is significantly higher for the downscaled analysis throughout the year, indicating better representation of daily precipitation variations in the downscaled analysis.

### *b. Detailed Regional Evaluation*

One of the advantages of global downscaling is that we can downscale any regional area over the globe. In this section North America and Japan, both rich in regional scale observations, are investigated.

#### **1) Validation over North America with North American Regional Reanalysis (NARR)**

In Figure 8, the monthly mean wind speed for July 2001 is compared with NARR (Mesinger et al., 2006). NARR is a data assimilation product using the 32 km resolution Eta model. The larger wind speed in most of the Pacific side of the

continent was reduced to the level of NARR in the downscaled analyses, particularly over Alaska and British Columbia, the west coast of the U.S., and Baja California. A similar reduction can also be seen in northern Texas and Oklahoma.

Figure 9 shows the deviation of daily mean 2-meter temperature from the monthly averages on July 29, 2001. Large-scale anomalies, such as the cold anomaly in western Canada, the Labrador Peninsula, and the west and east coasts of the U.S. and the warm anomaly in Alaska, Greenland, the central U.S. and Canada, are common in these three panels, but in R2 (Fig. 9a), cold regions appear more distinctively than those of NARR (Fig. 9c), such as in northern Mexico and the southern U.S. In the T248 downscaling (Fig. 9b), the distribution becomes more similar to that of NARR. The improvement is found consistently throughout the year, up to 0.2 K decrease of monthly averaged root mean square difference (Fig. 9d). The reason for the improvement is probably because the regions are characterized by complex geography, such as the Gulf of California, the Sierra Madres in northern Mexico and the Great Plains in the U.S., where the dominant scale is much smaller than the critical scale of 2000 km.

## **2) Validation over Japan with AMeDAS**

Next, we compared our results with more than 1000 Automated Meteorological Data Acquisition System (AMeDAS), in-situ meso-scale surface observatories covering all of Japan, for wind speed, humidity, temperature, and precipitation. The average AMeDAS station location interval is about 20 km, and most of the observations are hourly.

Table 2 shows the averages of correlation coefficient of the four surface variables between the downscaled analysis and AMeDAS in January and July 2001.

There is clearly a large improvement in January precipitation, and a somewhat smaller improvement in the temperature fields for both months. By averaging the coefficients over the region for all months, the wind speed, temperature, and precipitation of the downscaled analysis became closer to the AMeDAS observations than those of Reanalysis. Only the humidity fields stayed similar or became worse than R2, because humidity was not nudged and corrected in T248. Because the analysis of surface moisture plays an important role at the regional scales, improving the moisture field would make the whole simulation better.

In Figure 10, the temporal variations of the variables (a) wind speed, (b) temperature, (c) humidity, and (d) precipitation for the first 10 days in July 2001 at a single grid point at 140.0E and 36.0N (near Tsukuba, Japan) are shown. We see that the improvement of the correlation coefficient in Table 2 was from better reproduction of diurnal variations of wind speed and temperature. The diurnal cycle of absolute humidity is weak, but other fluctuations were better reproduced in the T248 downscaling. In precipitation, the downscaled analysis captured a rain event on 6 July, 2001, which was very sharp and short according to the observation, whereas R2 did not have any precipitation in that period.

### **3) Synoptic/Sub-synoptic Scale Weather Patterns**

In this section, several typical intense synoptic- and subsynoptic-scale atmospheric phenomena are selected and the downscaled analysis is compared with the corresponding coarse resolution Reanalysis. A Santa Ana wind event in Southern California, a Mistral in West Europe, and the katabatic wind in Antarctica are selected. Figure 11 shows daily snapshots of temperature anomaly (deviation from monthly mean), wind, and surface elevation of those events for R2 and the

downscaled analysis.

The Santa Ana is a warm, dry northeasterly wind in Southern California during fall and winter. Typical features of the Santa Ana can be found in many works (e.g., Hu and Liu, 2003). An event on January 3, 2001 is shown here. Both R2 (Fig.11a) and the downscaled analysis (Fig.11b) captured high temperatures along the coast of Southern California, but the downscaled analysis showed more detailed wind patterns associated with the complex topography of Sierra Nevada, whereas winds in R2 were more uniform.

The Mistral is a cold, strong northwesterly in southern France and Sardinia which occurs during winter to spring. Figure 11c and 11d show R2 and the downscaled winds and temperature on 22 December 2001, respectively. General characteristics of the phenomenon, such as the cold northwesterly in the southern coast of France, were captured in R2, but more detailed features, *i.e.*, colder and stronger northwesterlies which were more regionalized over the area from the western edge of the Alps to north of the Pyrénées, were found in the downscaled analysis,. It is noted that warm temperature anomalies in R2 in the middle of France, Germany and Switzerland disappeared in the downscaled analysis, due to the enhancement of cold anomalies in the southern part of France.

A katabatic wind is a prominent feature of the surface wind system over Antarctica. Figure 11e shows temperature and wind in R2 over the Antarctic Peninsula. The coastal katabatic winds are not apparent. In the downscaled analysis, however, prominent katabatic winds appear over the eastern coast of the peninsula. This difference looks quite remarkable. However, it should be mentioned that large-scale katabatic winds are already reasonably well simulated in

the coarse resolution reanalyses over flat terrain and slopes, such as over the coastline of Eastern Antarctica (Parish and Cassano, 2001), and the improvement in the downscaled analysis is not so significant over those areas. Since the width of the Antarctic Peninsula is at most 500 km with complex topography, the downscaling was capable of producing small-scale details that R2 could not represent.

#### **4. Summary and Conclusions**

In this study, an attempt has been made to develop a global version of dynamical downscaling using the global spectral model (GSM) with a spectral nudging technique. A modified version of the scale-selective bias correction (SSBC) (Kanamaru and Kanamitsu, 2007a) was applied. The global downscaling is free of the lateral boundary noise which contaminates regional downscaling, and is a way to produce computationally efficient high-resolution global reanalysis datasets from coarse resolution data assimilation analysis.

SSBC was modified for GSM in three different ways. First, the large-scale temperature of the scale greater than 2000 km was nudged at every Gaussian Latitude in addition to the zonal and meridional components of wind. This was necessary to reduce the large-scale temperature bias in the stratosphere in equatorial tropics. Second, the nudging of perturbation field was applied instead of the nudging of perturbation tendency. Large scale biases that can occur in the perturbation tendency nudging may not occur in the nudging of the perturbation itself. Third, humidity was not nudged or corrected. With this nudging scheme, large-scale features of the reanalysis were well maintained in the downscaling. The departures of geopotential height of downscaled analysis from reanalysis were in a

range of 5 to 10 meters at all of the pressure levels.

Using a T248L28 (about 50 km resolution) global model, downscaling was performed for the entire year of 2001, using T62L28 NCEP/NCAR R2 as a large-scale forcing. Surface variables and precipitation were compared with R2 and available high-resolution observations. The global temperature fields compared with CRU temperature showed that the downscaled analysis better matched with observation due to the better topography. Monthly averaged precipitation, its seasonality and daily variation were compared with those of CRU and GPCP. The daily variability in the downscaled precipitation was better reproduced in the downscaled analysis than in the R2 throughout the year.

Comparisons with NARR over North America showed that the downscaled surface wind speed and temperature are closer to NARR than the Reanalysis to NARR. Over Japan, the comparison with more than 1000 AMeDAS in-situ observations showed that the downscaled analysis fits better to observation than R2 for surface temperature, wind speed, and precipitation. The fit of humidity was not significantly improved. The improvement of diurnal variation of surface temperature was significant.

In addition, three typical synoptic/sub-synoptic scale weather features were selected for comparison, namely the Santa Ana in Southern California, the Mistral in Southern France, and katabatic winds in Antarctica. The global downscale clearly showed realistic regional-scale features with respect to temperature and wind.

One of the purposes of this study is to determine whether this global downscaling can serve as a replacement of the global high-resolution reanalysis

without performing an expensive high-resolution global data assimilation. From the present result, this seems to be the case at least for surface meteorological variables and precipitation. However, in order to confirm this, it is also necessary to investigate the fit of the downscaling to observations in the free atmosphere and to compare the results with the high-resolution data assimilation analysis. Since this would require a full objective analysis system capable of using high-density surface observation, it is beyond our capability at this time.

### **Acknowledgments:**

A part of this research was funded by the Japan Society for the Promotion of Science Postdoctoral Fellowships for Research Abroad. Additionally, this work was funded by the California Energy Commission Public Interest Energy Research (PIER) program, which supports the California Climate Change Center. The authors thank G. Franco for his assistance in performing the research. This study was also partially supported by NSC 95-211-M133 -001 -AP4 and NOAA NA17RJ1231. The views expressed herein are those of the authors and do not necessarily reflect the views of NOAA. We would like to thank two anonymous reviewers and Drs. H. Kanamaru, J. Roads, and V. Misra for their constructive comments, Ms. C. Papadopoulos for her technical help with computational resources, and Ms. D. Boomer for her assistance in proof-reading.

## APPENDIX A

### Sensitivity Experiments of the Nudging Method and Parameters

Some additional experiments were performed using the same model configurations as those described in Section 2 for evaluating sensitivities of the nudging scale  $L$  and the weighting coefficient  $\alpha$ . Experiments similar to CTL and TEMP but with  $L=1000$  km are named L1000 and L1000T, respectively. Experiments similar to TEMP with different  $\alpha$ , namely  $\alpha=0.5$  and  $2.0$ , are named as ALP05, and ALP2, respectively. Experiments that nudge the coefficients of spherical harmonics function instead of those of the zonal Fourier series are named SP21 and SP42, denoting different nudging scale by wave number  $N=21$  (about 2000 km) and  $N=42$  (about 1000 km), respectively.

As shown in Table 1 in the main text, the sensitivities of downscaling to both  $L$  and  $\alpha$  are not significant. The comparison between CTL and L1000 and between TEMP and L1000T indicates that the result of the 2000 km nudging scale was sufficiently similar to that of 1000 km. The 2000 km scale was chosen as our default considering the accuracy of Reanalysis data over ocean and tropics as noted in the main text. As to the form of the nudging coefficients, ALP2 was almost identical to TEMP and ALP05 was worse than TEMP, implying that it is difficult to significantly decrease the RMSD by adjusting the constant nudging coefficient. SP21 is about 2000 km nudging scale, but it was worse than NoQ, indicating that nudging in the north-south direction should be stronger than that in the east-west direction. SP42, which is 1000 km scale nudging, was similar to NoQ. These results indicate that the zonal spectral nudging was slightly more effective than the horizontally uniform-scale nudging because of the heterogeneous characteristics of

the large scale atmosphere.

## REFERENCES

- Caplan, P., J. Derber, W. Gemmil, S.-Y. Hong, H.-L. Pan and D. Parrish, 1997: Changes to the 1995 NCEP operation medium-range-forecast model analysis-forecast system, *Weather Forecast*, **12**, 581-594.
- Dirmeyer, P.A., X. Gao, M. Zhao, T. Oki, N. Hanasaki, 2006: The second global soil wetness project (GSWP-2), *Bull. Amer. Meteor. Soc.*, **87**, 1381-1397.
- European Regional Reanalysis project (EURRA), 2005: Meeting Report on Workshop to discuss a potential European Regional Reanalysis project (EURRA).
- Fuhrer, J., M. Beniston, A. Fischlin, Ch. Frei, S. Goyetter, K. Jasper, Ch. Pfister, 2006: Climate risks and their impact on agriculture and forests in Switzerland, *Climatic Change*, **79**, 79-102.
- Ghan, S.J., T. Shippert, and J. Fox, 2006: Physically based global downscaling: regional evaluation, *J. Climate*, **19**, 429-445.
- Hu, H. and T. Liu, 2003: Oceanic thermal and biological responses to Santa Ana winds, *Geophys. Res. Lett.*, **30**, 1596, doi:10.1029/2003GL017208.
- Huffman, G.J., R.F. Adler, M.M. Morrissey, D.T. Bolvin, S. Curtis, R. Joyce, B. McGavock, and J. Susskind, 2001: Global precipitation at one-degree daily resolution from multisatellite observation, *J. Hydromet.*, **2**, 36-50.
- Iacobellis, S.F., and R.C.J. Somerville, 2000: Implications of Microphysics for Cloud-Radiation Parameterizations: Lessons from TOGA COARE, *J. Atmos. Sci.*, **57**, 161-183.
- Juang, H.-M.H, S.-Y. Hong, and M. Kanamitsu, 1997: The NCEP regional spectral model: an update, *Bull. Amer. Meteor. Soc.*, **78**, 2125-2143.
- Kain, J.S. and J. M. Fritsch, 1990: A One-Dimensional Entraining/Detraining Plume

- Model and Its Application in Convective Parameterization, *J. Atmos. Sci.*, **47**, 2784-2802.
- Kanamaru, H. and M. Kanamitsu, 2007a: Scale-selective bias correction in a downscaling of global analysis using a regional model, *Mon. Wea. Rev.*, **135**, 334-350.
- Kanamaru, H., and M. Kanamitsu, 2007b: Dynamical downscaling of global analysis/simulation over the Northern Hemisphere, submitted to *Mon. Wea. Rev.*
- Kanamitsu, M., H. Kanamaru, Y. Cui and H. Juang. 2005: Parallel implementation of the Regional Spectral Atmospheric Model. CEC-500-2005-014. Available from <http://www.energy.ca.gov/2005publications/CEC-500-2005-014/CEC-500-2005-014.PDF>.
- Kanamitsu, M., W. Ebisuzaki, J. Woolen, J. Potter, and M. Fiorino, 2002: NCEP/DOE AMIP-II Reanalysis (R-2), *Bull. Amer. Meteor. Soc.*, **83**, 1631-1643.
- Koshyk, J.N. and K. Hamilton, 2001: The horizontal kinetic energy spectrum and spectral budget simulated by a high-resolution troposphere-stratosphere-mesosphere GCM, *J. Atmos. Sci.*, **58**, 4, 329-348.
- Lehner B., P. Döll, J. Alcamo, T. Henrichs, F. Kaspar, 2006: Estimating the Impact of Global Change on Flood and Drought Risks in Europe: A Continental, Integrated Analysis, *Climatic Change*, **75**, 273-299.
- Meinke, I., J. Roads, and M. Kanamitsu, 2007: Global evaluation of the RSM simulated precipitation through transferability studies during CEOP, *J. Meteor. Soc. Japan*, in print.

- Mesinger, F., and co-authors, 2006: North American regional reanalysis, *Bull. Amer. Meteor. Soc.*, **87**, 343-360.
- Miller, N.L., K.E. Bashford, and E. Strem, 2003: Potential impacts of climate change on California hydrology, *J. Amer. Water Resour. Assoc.*, **39**, 771-784.
- Mitchell, T.D. and P.D. Jones, 2005: An improved method of constructing a database of monthly climate observations and associated high-resolution grids, *Int. J. Climatol.*, **25**, 693-712.
- Moorthi, S., and M.J. Suarez, 1992: Relaxed Arakawa-Schubert: a parameterization of moist convection for general circulation models, *Mon. Wea. Rev.*, **120**, 978-1002.
- Oki, T., and S. Kanae, 2006: Global hydrological cycles and world water resources, *Science*, **313**, no.5790, 1068-1072.
- Pan, H.-L. and W.-S. Wu, 1994: Implementing a mass flux convective parameterization package for the NMC medium-range forecast model, Preprints, 10<sup>th</sup> Conf. on Numerical Weather Prediction, Portland, OR, Amer. Meteor. Soc., 96-98.
- Parish, T.R. and J.J. Cassano, 2001: Forcing of the wintertime Antarctic boundary layer winds from the NCEP-NCAR global reanalysis, *J. Appl. Meteor.*, **40**, 810-821.
- Rockel, B., I. Meinke, J. Roads, W.J. Gutowski, Jr., R.W. Arritt, E.S. Takle, C. Jones, 2005: The inter-CSE Transferability study, *CEOP Newsletter*, **8**, 4-5.
- von Storch, H., H. Langenberg, and F. Feser, 2000: A spectral nudging technique for dynamical downscaling purposes, *Mon. Wea. Rev.*, **128**, 3664-3673.
- Wilby, R.L., L.E. Hay, and G.H. Leavesley, 1999: A comparison of downscaled and

raw GCM output: implications for climate change scenarios in the San Juan river basin, Colorado, *J. Hydrol.*, **225**, 67-91.

## Figure Captions

Figure 1: Power spectra of kinetic energy at two different sigma levels. (a)  $\sigma=0.864$ : low troposphere and (b)  $\sigma=0.147$ : high troposphere. Black dashed lines indicate Reanalysis 2 (R2), blue solid lines are forecast simulation (FCST), and red dotted, green dotted, and black solid lines indicate CTL, TEMP1, and TEMP2, respectively. Gray lines indicate  $-3$  (dashed) and  $-5/3$  (dotted) slopes for comparison. All spectra are averaged for 5 days from 6 March 1990.

Figure 2: Difference of 50hPa geopotential height between the control (CTL) and Reanalysis 2 (R2). The result is 3-day averaged from 6 Mar 1990.

Figure 3: Global RMSD of geopotential height at 17 pressure levels for CTL (dotted line with closed squares), TEMP (solid line with open squares), and NoQ (solid gray line with crosses), compared with R2. The result is 3-day averaged from 6 Mar 1990.

Figure 4: Global monthly mean air temperature at 2 meter surface over land in July 2001. (a) CRU observation, (b) Reanalysis 2, and (c) T248 simulation. Differences from CRU (a) of R2 and T248 are shown in (d) and (e), respectively. The differences are rendered in CRU's resolution (0.5 degree).

Figure 5: Global distribution of monthly precipitation in January (left column) and July (right column) 2001. The top panels (a, b) are CRU, the next panels (c, d) show GPCP, then R2 (e, f), T248 nudged simulation results are shown (g, h), and finally T248 forecast simulation results (i, j).

Figure 6: Seasonality of global averaged precipitation, over whole (a) globe and (b) land. GPCP is used in (a), and CRU is used in (b). Black solid lines with circles are assigned for both observations. Dashed lines with triangles and dotted

lines with squares indicate R2 and T248, respectively.

Figure 7: Correlation coefficient of R2 and T248 daily precipitation with GPCP are globally averaged in each month. A solid line with circles and a dotted line with squares indicate Reanalysis 2 and T248, respectively.

Figure 8: Monthly mean surface wind speed at 10 m over North America. (a) Reanalysis 2, (b) T248, and (c) NARR are shown for July 2001.

Figure 9: Daily mean surface temperature anomaly from monthly average over North America. (a) Reanalysis 2, (b) T248, and (c) NARR are shown for 29 July 2001.

Figure 10: Temporal variations of Reanalysis 2 (thin solid line with open square), T248 (black thick line with closed circle), and AMeDAS observation (gray thick line) are compared for (a) surface wind speed, (b) surface temperature, (c) surface humidity, and (d) precipitation.

Figure 11: Daily averaged temperature anomalies (shades), winds (arrows), and topography (gray contour; 300 m interval and 0 m line are omitted). Left and right columns show Reanalysis 2 with linear interpolation to the same resolution with T248 and T248-nudged run, respectively. (a, b) Santa Ana wind in Southern California on 3 January 2001, (c, d) Mistral wind in West Europe on 22 December, 2001, and (e, f) katabatic winds in Antarctic Peninsula on 29 July 2001 are shown. Number of arrows is horizontally cropped to 1/4 in (f).

Table 1. Specification of preliminary T126 experiments

	Zonal Correction	Spectral Nudging	Weighting Coefficient ( $\alpha$ )	Nudging Scale ( $L$ )	500Z rmsd (m) <sup>a</sup>	Precip (mm/day) <sup>b</sup>
FCST	None	None	---	---	73.4	3.32
CTL	TQ	UV	0.9	2000 km	9.9	3.42
TEMP	Q	UV and T	0.9	2000 km	6.1	3.55
NoQ	None	UV and T	0.9	2000 km	6.0	3.03
L1000	TQ	UV	0.9	1000 km	9.0	3.36
L1000T	Q	UV and T	0.9	1000 km	4.3	3.44
ALP05	Q	UV and T	0.5	2000 km	6.5	3.88
ALP2	Q	UV and T	2.0	2000 km	5.8	4.36
SP21	None	UV and T	0.9	T21 Spec <sup>c</sup>	10.2	3.08
SP42	None	UV and T	0.9	T42 Spec <sup>d</sup>	5.6	3.12

a: global RMSD for geopotential height at 500 hPa with R2 for 6-9 Mar 1990

b: global average of precipitation for 6-9 Mar 1990

c: equivalent with about 2000 km zonal nudging scale

d: equivalent with about 1000 km zonal nudging scale

Table 2. Averaged correlation coefficient with AMeDAS data over Japan

	January 2001		July 2001	
	R2	T248	R2	T248
Wind speed	0.47	0.48	0.28	0.35
Temperature	0.74	0.78	0.68	0.80
Humidity	0.81	0.79	0.66	0.53
Precipitation	0.32	0.61	0.13	0.14

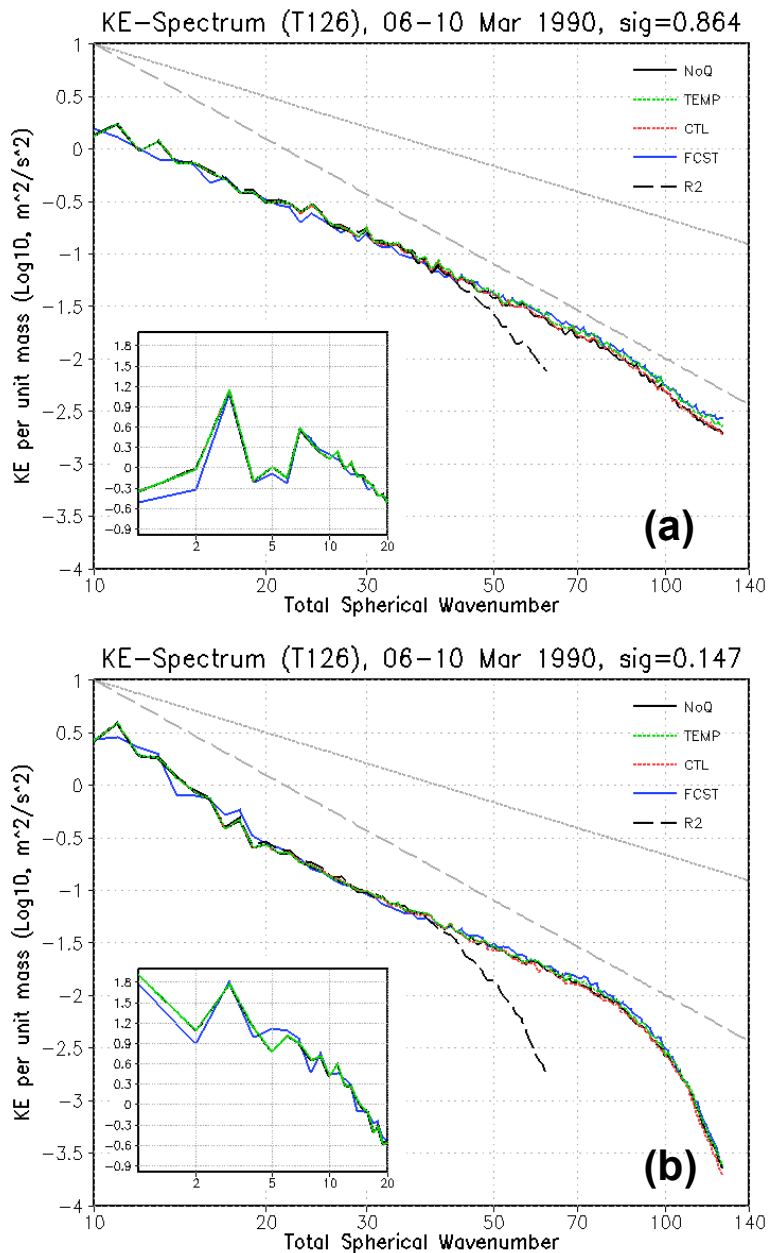


Figure 1: Power spectra of kinetic energy at two different sigma levels. (a)  $\sigma=0.864$ : low troposphere and (b)  $\sigma=0.147$ : high troposphere. Black dashed lines indicate Reanalysis 2 (R2), blue solid lines are forecast simulation (FCST), and red dotted, green dotted, and black solid lines indicate CTL, TEMP1, and TEMP2, respectively. Gray lines indicate  $-3$  (dashed) and  $-5/3$  (dotted) slopes for comparison. All spectra are averaged for 5 days from 6 March 1990.

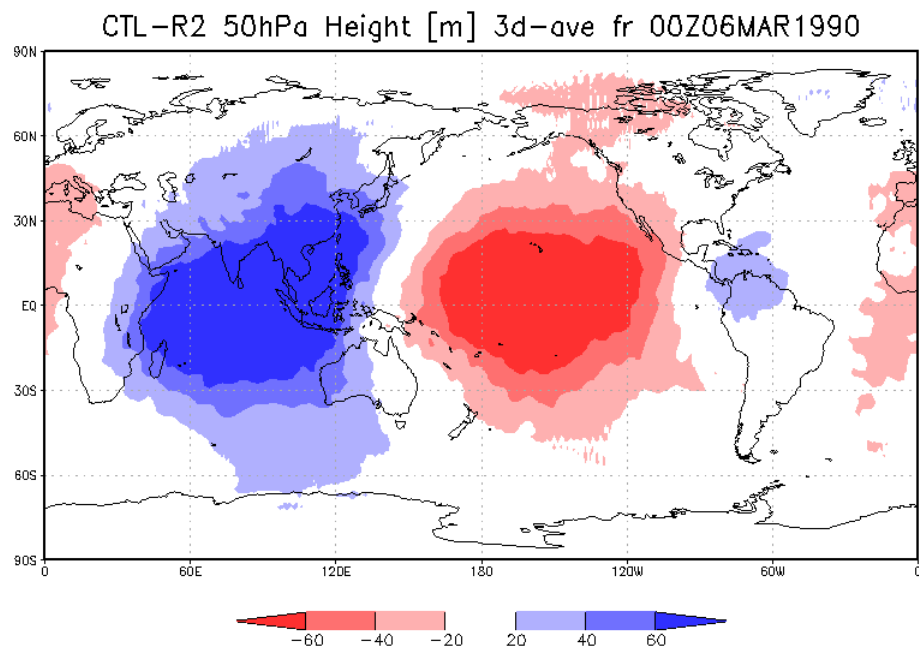


Figure 2: Difference of 50hPa geopotential height between the control (CTL) and Reanalysis 2 (R2). The result is 3-day averaged from 6 Mar 1990, in R2's 2.5-degree resolution.

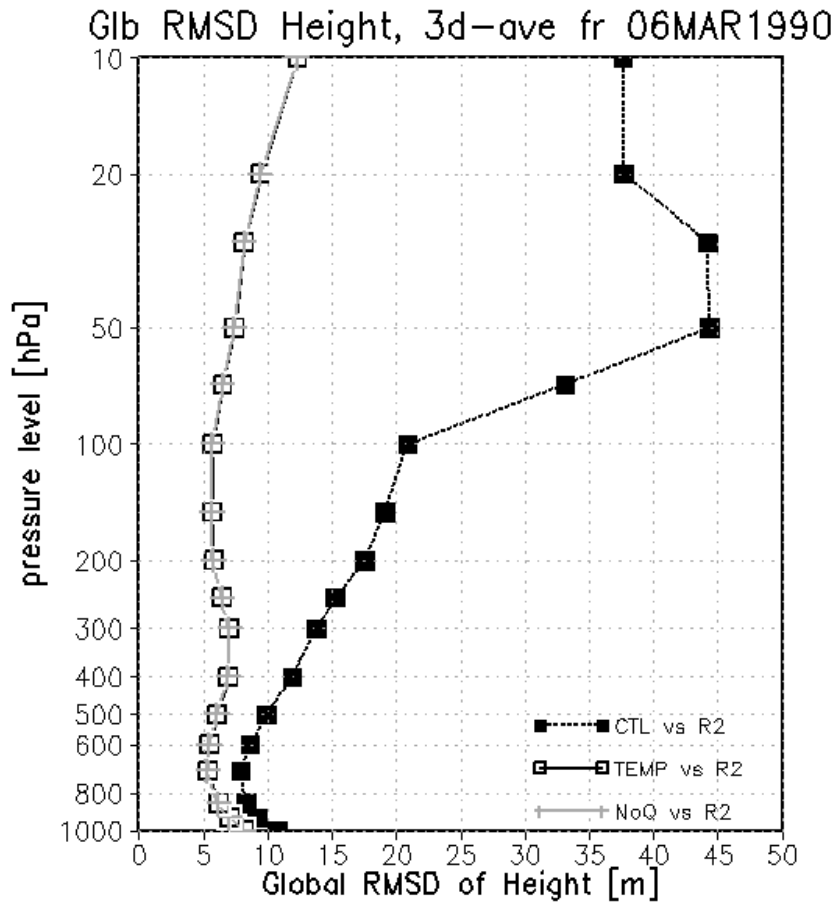


Figure 3: Global RMSD of geopotential height at 17 pressure levels for CTL (dotted line with closed squares), TEMP (solid line with open squares), and NoQ (solid gray line with crosses), compared with R2. The result is 3-day averaged from 6 Mar 1990.

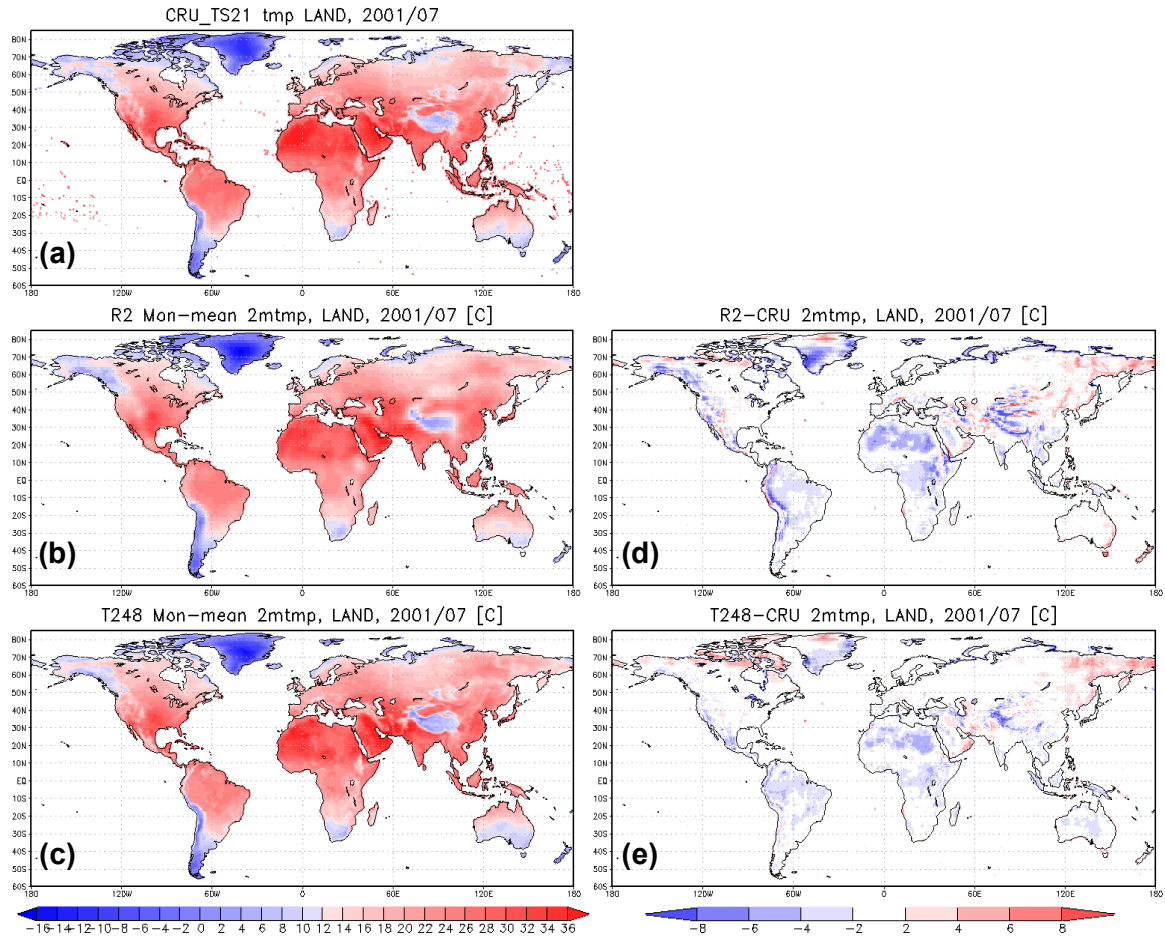


Figure 4: Global monthly mean air temperature at 2 meter surface over land in July 2001. (a) CRU observation, (b) Reanalysis 2, and (c) T248 simulation. Differences from CRU (a) of R2 and T248 are shown in (d) and (e), respectively. The differences are rendered in CRU's resolution (0.5 degree).

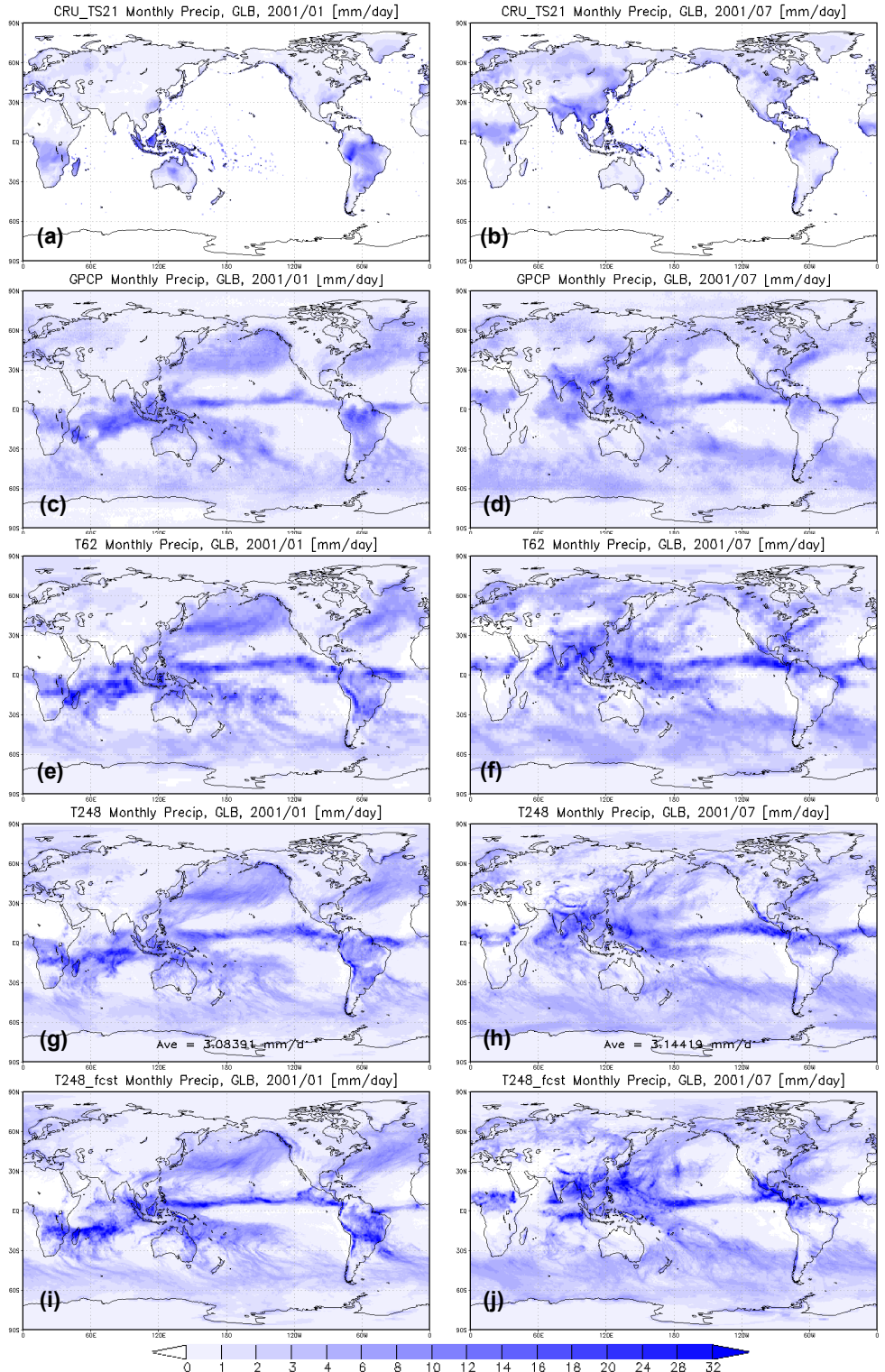


Figure 5: Global distribution of monthly precipitation in January (left column) and July (right column) 2001. The top panels (a, b) are CRU, the next panels (c, d) show GPCP, then R2 (e, f), T248 nudged simulation results are shown (g, h), and finally T248 forecast simulation results (i, j).

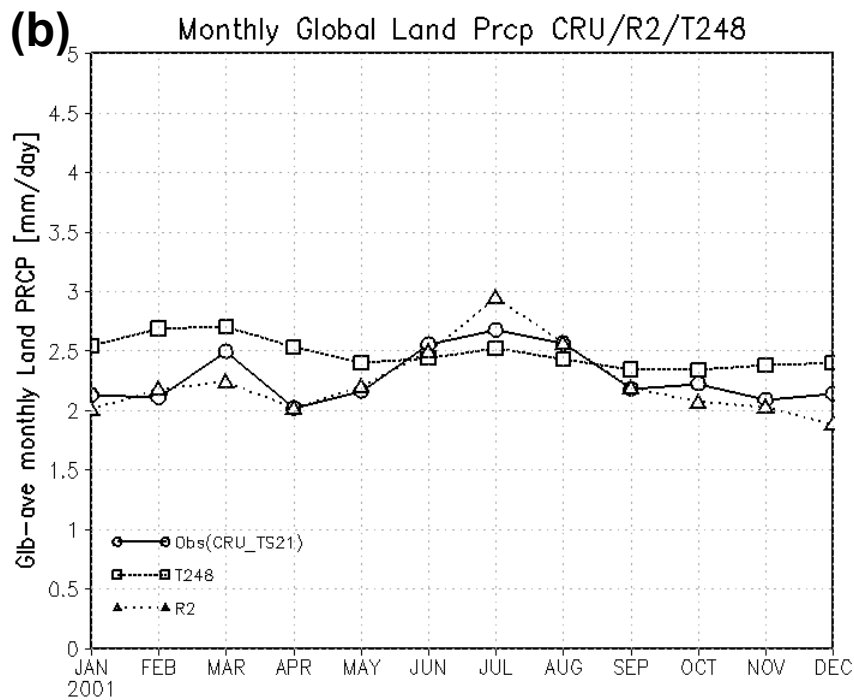
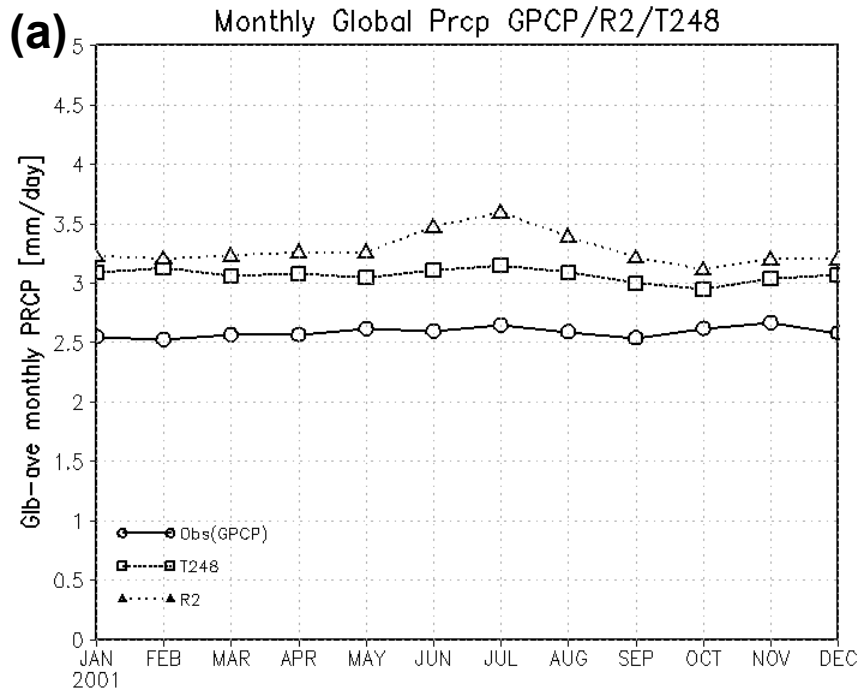


Figure 6: Seasonality of global averaged precipitation, over whole (a) globe and (b) land. GPCP is used in (a), and CRU is used in (b). Black solid lines with circles are assigned for both observations. Dashed lines with triangles and dotted lines with squares indicate R2 and T248, respectively.

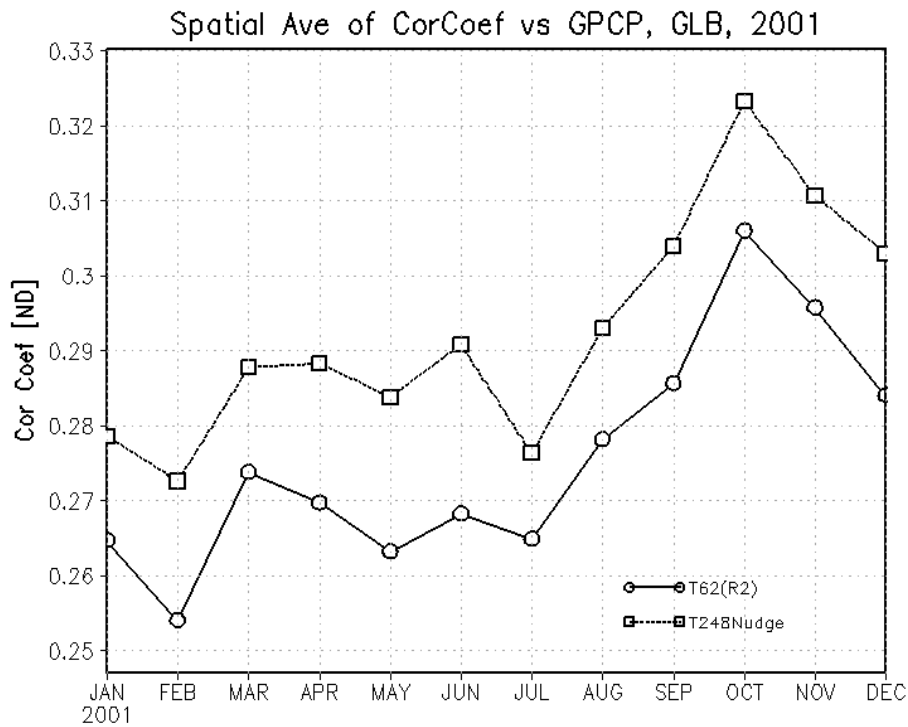


Figure 7: Correlation coefficient of R2 and T248 daily precipitation with GPCP are globally averaged in each month. A solid line with circles and a dotted line with squares indicate Reanalysis 2 and T248, respectively. The correlations are calculated on GPCP's 1-degree resolution.

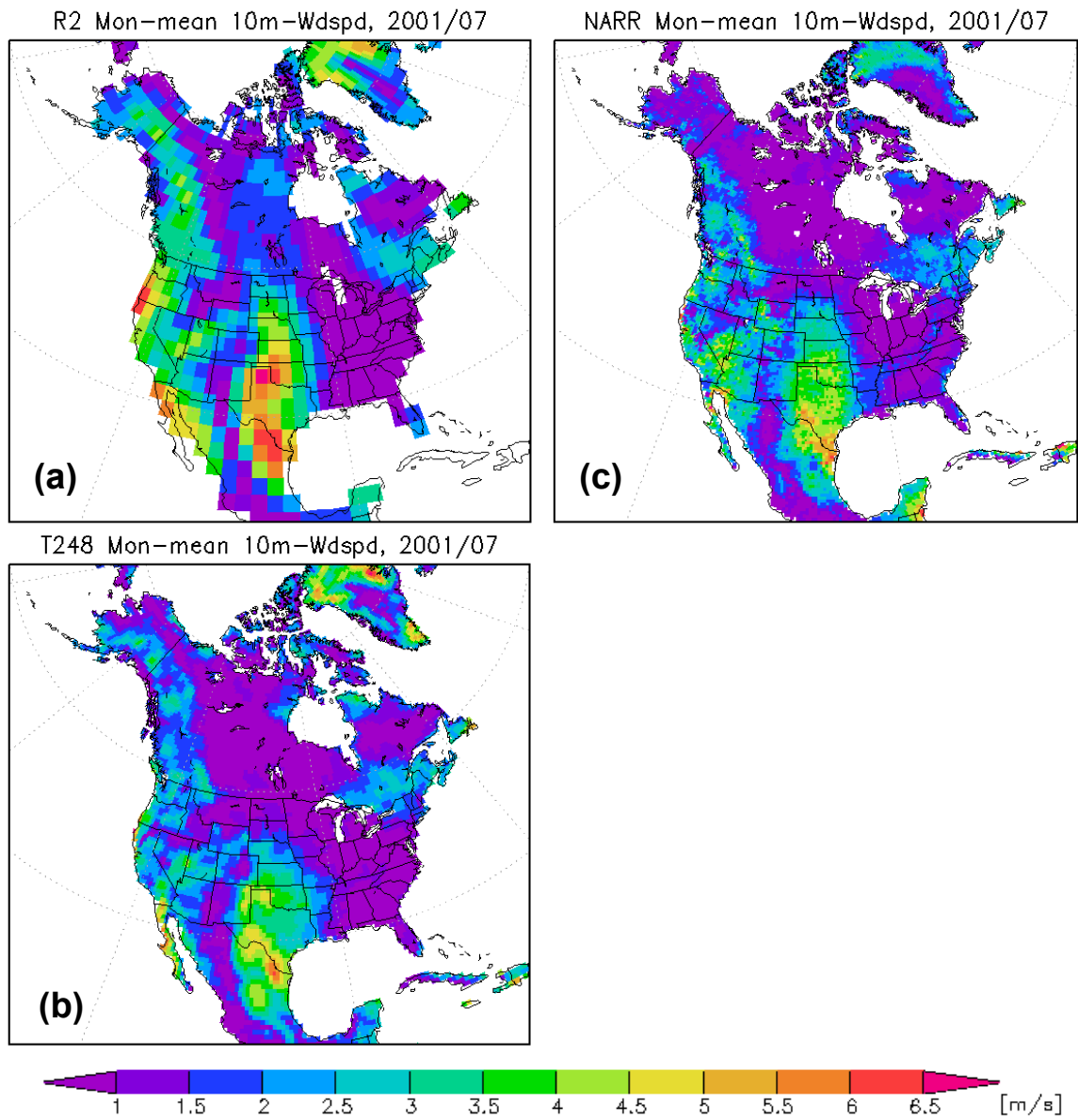
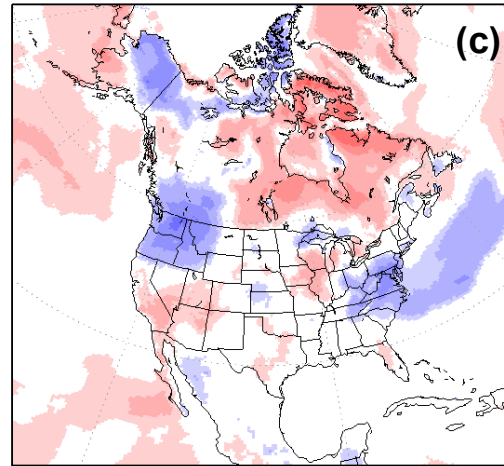
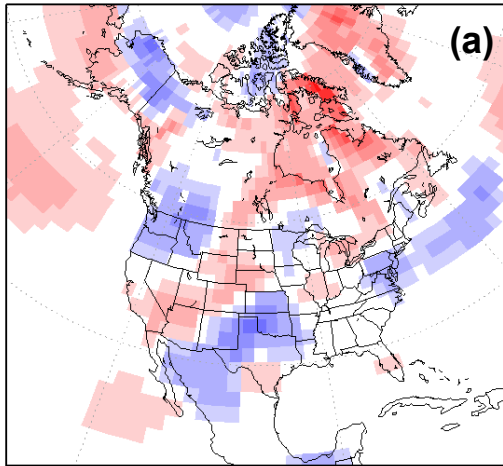


Figure 8: Monthly mean surface wind speed at 10 m over North America. (a) Reanalysis 2, (b) T248, and (c) NARR are shown for July 2001.

R2 Daymean-Monmean 2mtmp [K], 2001/07/29      NARR Daymean-Monmean 2mtmp [K], 2001/07/29



T248 Daymean-Monmean 2mtmp [K], 2001/07/29

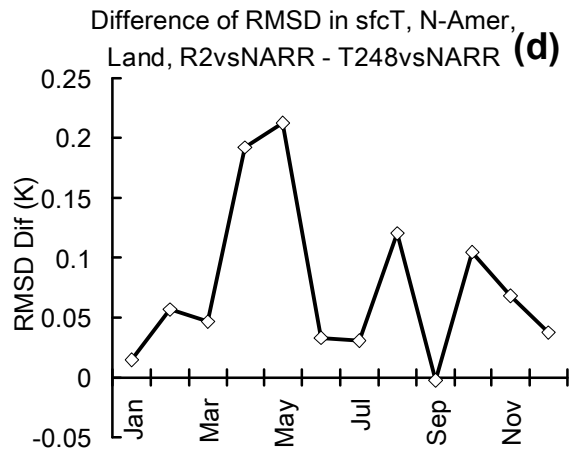
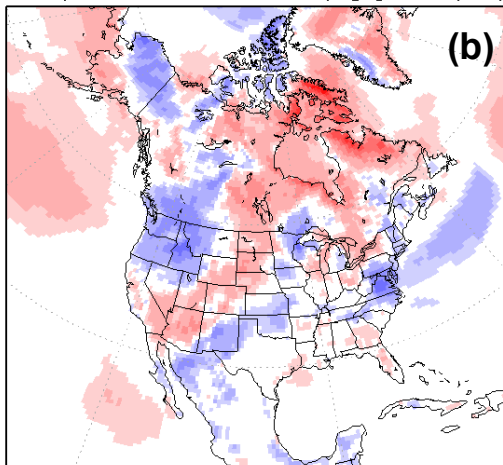


Figure 9: Daily mean surface temperature anomaly from monthly average over North America. (a) Reanalysis 2, (b) T248, and (c) NARR are shown for 29 July 2001. In (d) monthly means differences between area-averaged root mean square differences of the surface temperature anomaly with NARR (*i.e.*, RMSD between (b) and (c) minus that between (a) and (c)) are shown.

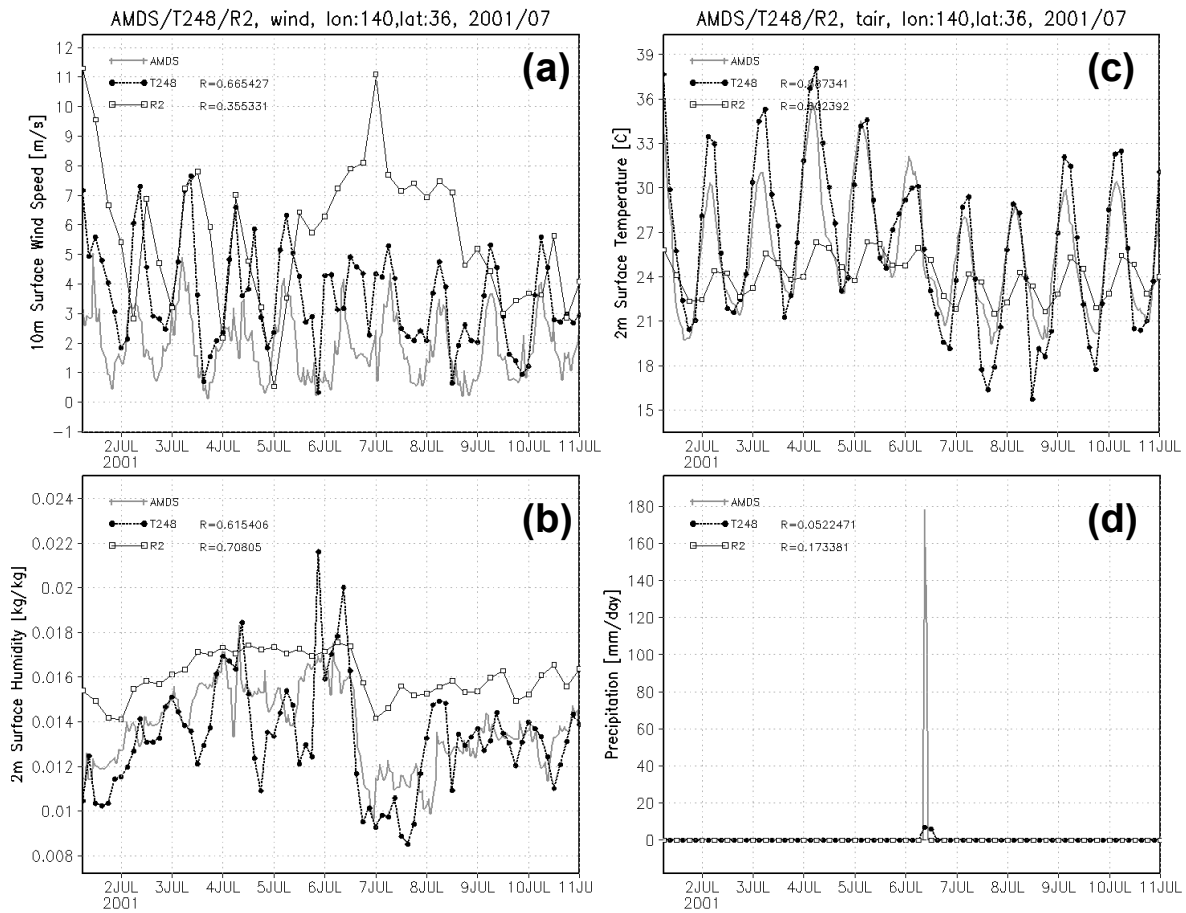


Figure 10: Temporal variations of Reanalysis 2 (thin solid line with open square), T248 (black thick line with closed circle), and AMeDAS observation (gray thick line) are compared for (a) surface wind speed, (b) surface temperature, (c) surface humidity, and (d) precipitation.

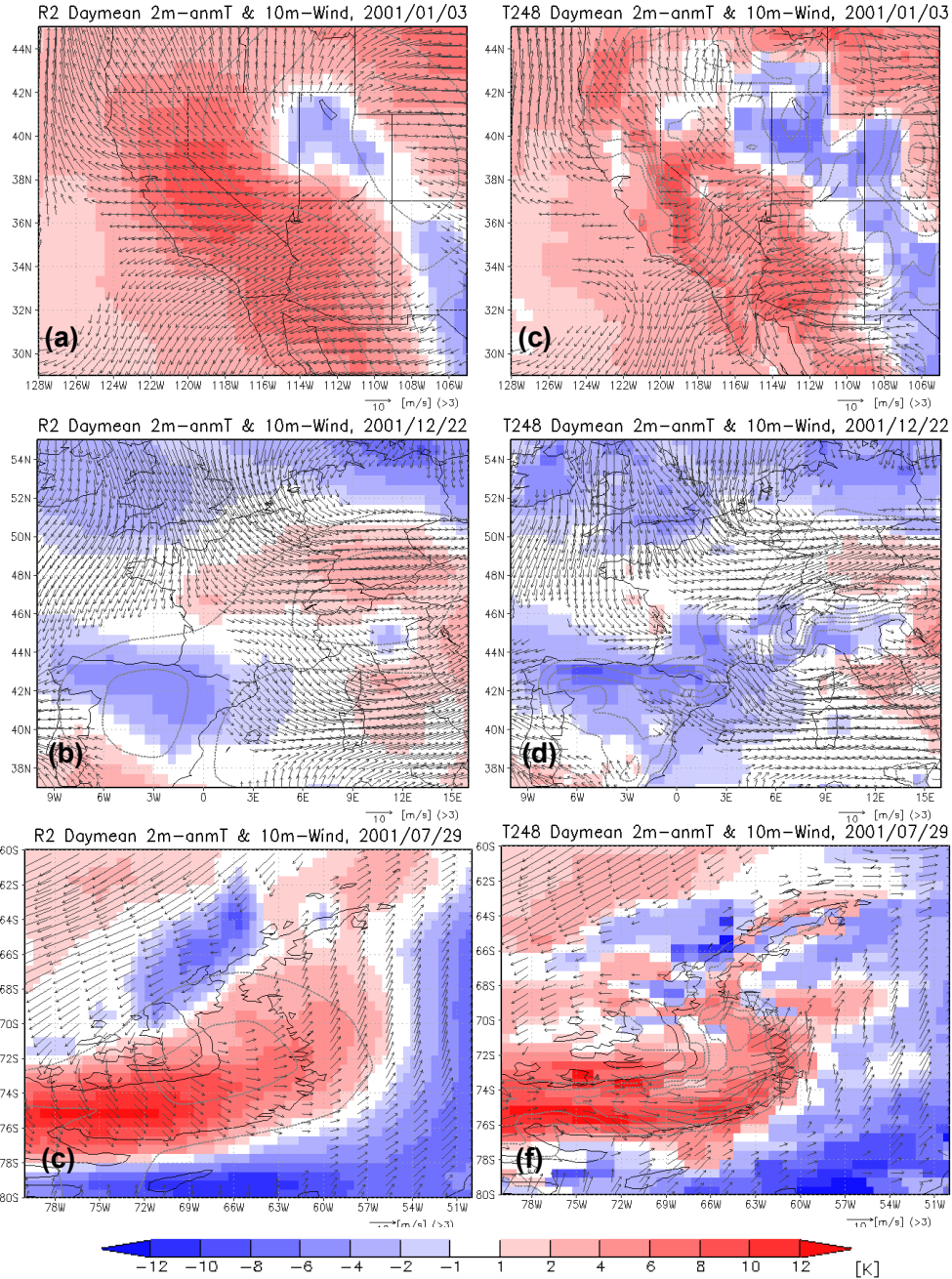


Figure 11: Daily averaged temperature anomalies (shades), winds (arrows), and topography (gray contour; 300 m interval and 0 m line are omitted). Left and right columns show Reanalysis 2 with linear interpolation to the same resolution with T248 and T248-nudged run, respectively. (a, b) Santa Ana wind in Southern California on 3 January 2001, (c, d) Mistral wind in West Europe on 22 December, 2001, and (e, f) katabatic winds in Antarctic Peninsula on 29 July 2001 are shown. Number of arrows is horizontally cropped to 1/4 in (f).